Poly(A) RNA Codistribution with Microfilaments: Evaluation by In Situ Hybridization and Quantitative Digital Imaging Microscopy

Krishan L. Taneja,* Lawrence M. Lifshitz,‡ Fredric S. Fay,‡ and Robert H. Singer*

Departments of *Cell Biology and ‡Physiology and the Biomedical Imaging Facility, University of Massachusetts Medical Center, Worcester, Massachusetts 01655

Abstract. The distribution of poly(A) RNA has been visualized in single cells using high-resolution fluorescent in situ hybridization. Digital imaging microscopy was used to quantitate the signal in various cellular compartments. Most of the poly(A) signal remained associated with the cellular filament systems after solubilization of membranes with Triton, dissociation of ribosomes with puromycin, and digestion of non-poly(A) RNA with ribonuclease A and T_1. The actin filaments were shown to be the predominant cellular structural elements associating with the poly(A) because low doses of cytochalasin released about two-thirds of the poly(A). An approach to assess the extent of colocalization of two images was devised using in situ hybridization to poly(A) in combination with probes for ribosomes, membranes, or F-actin. Digital imaging microscopy showed that most poly(A) spatially distributes most significantly with ribosomes, slightly less with F-actin, and least of all with membranes. The results suggest a mechanism for anchoring (and perhaps moving) much of the cellular mRNA utilizing the interaction between actin filaments and poly(A).

THE nucleic acids in the cell are organized in a spatially coherent manner. Evidence suggests that the DNA is nonrandomly positioned within the nucleus (Manuelidis et al., 1982; Lawrence et al., 1988), that the RNA transcribed from genes does not diffuse but is contained spatially along "tracks" which proceed toward the nuclear envelope (Lawrence et al., 1989). Once out of the nucleus, mRNA can be spatially organized within different cellular regions (Lawrence and Singer, 1986).

By what mechanisms might specific nucleic acid information be transduced into spatial information? Clearly, to maintain spatial order of the nucleic acids, they must be transported correctly throughout the cell and random diffusion minimized. Structural elements of the cell most likely anchor these molecules. Evidence over the last few decades indicates that mRNA is not free to diffuse within the cytoplasm but is bound to cellular structural elements ("the cytoskeleton") (Lenk et al., 1977). Components of the cytoskeleton implicated in the binding of mRNA or ribosomes (reviewed in Nielson et al., 1983; Hesketh et al., 1991) include microfilaments (Howe and Hershey, 1984; Ramaekers et al., 1983; Toh et al., 1980; Adams et al., 1983; Singer et al., 1989), intermediate filaments (Zumbe et al., 1982), and microtrabeculae (Wolosewick and Porter, 1979). The structural site to which the mRNA is tethered is unknown.

Address all correspondence to Robert H. Singer.

Furthermore, the site on the mRNA which interacts with cytoskeletal elements is likewise unknown. A good candidate for a direct attachment site would be the poly(A) which is present at the 3′ end of almost all eukaryotic mRNA (Sheiness and Darnell, 1973; Karpetsky et al., 1979; Brawerman, 1981). An alternate possibility is that some, or most, mRNA could be associated with the cytoskeleton through nascent protein chains (Isaacs and Fulton, 1987), or ribosomes (Howe and Hershey, 1984).

Hence, very little is known about the structural basis of cell–nucleic acid interactions. Almost all work assessing mRNA–cytoskeletal interactions has been based on cell fractionation and subsequent biochemical analysis, but the spatial distribution of the population of mRNAs and their association with specific filamentous proteins has never been visualized within single cells. To determine the spatial relationship between mRNA and cell structure we have colocalized poly(A) sequences on mRNA with cytoskeletal filaments using immunofluorescence to detect a hybridized, biotinated poly dT probe simultaneously with cytoskeletal proteins. Most importantly, quantitation of poly(A) codistribution with various cellular compartments was done using digital imaging microscopy. This approach provided the means to assess the amount of poly(A) associated with the nucleus, ribosomes, membranes, or various filament systems, and the significance of the codistribution. Furthermore, it allowed quantitation of the effects of treatments to

disrupt protein synthesis or filament systems, or of ribonuclease treatment on the retention of poly(A) within the cell. We have found that poly(A) RNA is distributed nonuniformly throughout the cell sequestered within various subcompartments of the nucleus and the cytoplasm. We provide evidence that much of the cytoplasmic poly(A) may be either directly or indirectly attached to actin filaments. This suggests a mechanism by which mRNA can be spatially positioned within the cell.

Materials and Methods

Cell Culture

Human diploid fibroblast cells were plated at a density of 10^5 cells per 100-mm^2 dish containing autoclaved gelatin-coated coverslips in Dulbecco's Minimal Essential Medium (DMEM), low glucose supplemented with 10% FBS. To fix cells, the coverslips were washed in HBSS and immersed in 4% paraformaldehyde in PBS (2.7 mM KCl, 1.5 mM KH_2PO_4, 0.137 M NaCl, and 8 mM Na_2HPO_4, pH 7.5) containing 5 mM $MgCl_2$ for 15 min at room temperature. After fixation cells were washed twice with 70% ethanol and stored in 70% ethanol at 4°C.

Preparation and Labeling of Oligonucleotide Probe

Poly dT (55 bases) and poly dA (55 bases) were synthesized and purified by PAGE. For 3'-end labeling, probe (25 pM) in 50 μl was incubated with 25 μM of bio-16-dUTP (BMB), 140 mM potassium cacodylate, 30 mM Tris-HCl, pH 7.6, 1 mM $CoCl_2$, 0.1 mM DTT, and 100 U terminal transferase (BMB) at 37°C for 60 min. For 5'-end labeling, 5 pM of probe was incubated at 37°C for 60 min with 100 μCi of ^{32}p-γ-ATP (>3,000 Ci/mM) (Amersham Corp., Arlington Heights, IL) in 20 μl volume containing 25 mM $MgCl_2$, 25 mM β-mercaptoethanol, 175 mM Tris-HCl, pH 7.5, and 20 U of T_4 polynucleotide kinase (Amersham Corp.). The reaction products were purified by gel filtration on 1 × 20-cm G-50 sephadex column.

Preparation of Nick-Translated Probe

A pBR322 plasmid containing chick β-actin cDNA (Cleveland et al., 1980) and one containing chick α-tubulin cDNA (Cleveland et al., 1980; Valenzuela et al., 1981) were mixed in equal amounts, DNA (0.5 μg) was nick translated in 30 μl containing 50 mm Tris, pH 7.2: 10 mM $MgSO_4$; 0.1 mm DTT; 60 μm each of dATP, dTTP, dGTP; 100 pM of αp^{32} dCTP (800 Ci/mmole); DNAse 0.2 μg and DNA polymerase 10 U for 2 h at 16°C. Nick-translated product was purified over sephadex G-50 column, the specific activity was ~2 × 10^8 cpm/μg.

Hybridization and Detection

5 ng of the probe was dried with *E. Coli* tRNA (10 μg) and sonicated salmon sperm DNA (10 μg) and then suspended in 10 μl of 30% formamide containing 20 mM sodium phosphate, pH 7.0. Before hybridization, the probe was mixed with 10 μl of hybridization buffer with a final concentration of the probe 250 ng/ml in 15% formamide, 10% dextran sulfate, 2× SSC (.3 M NaCl, .03 M citric acid, pH 7.0), 0.2% BSA, 10 mM sodium phosphate, pH 7.0, and .5 mg/ml each of *E. Coli* tRNA and salmon sperm DNA. Fixed cells were rehydrated in PBS plus 5 mM $MgCl_2$ for 10 min and prehybridized in 15% formamide, 2× SSC and 10 mM sodium phosphate, pH 7.0, at room temperature for 10 min. The coverslips were placed cell side down on parafilm containing 20 μl of hybridization mix and incubated at 37°C for 2–3 h in a humidified incubator. After hybridization coverslips were washed successively 30 min each with 15% formamide, 2× SSC, 10 mM sodium phosphate, pH 7.0, at 37°C; twice with 15% formamide, 1× SSC, 10 mM sodium phosphate, pH 7.0, at 37°C; and twice with 1× SSC at room temperature. After hybridization and washing, the coverslips were rinsed in 4× SSC, 0.01% Triton for 5 min, then were incubated with Texas red-avidin (2.5 μg/ml) or with fluorescein-avidin (10 μg/ml) in 4× SSC, 1% BSA for 45 min at room temperature. The coverslips were washed twice with 4× SSC, 0.01% Triton for 10 min each at room temperature and once with PBS for 5 min at room temperature. The coverslips were mounted on the slides in DABCO (2.3 mg of DABCO in 50% glycerol in PBS) containing DAPI or propidium iodide.

Triton Extraction

The coverslips containing cells were washed with HBSS to remove the medium and with cold CSK buffer (0.3 M sucrose, 0.1 M KCl, 5 mM $MgCl_2$, 10 mM Pipes, pH 6.9, 2 mM EGTA, 1.2 mM PMSF, 2 mM vanadyl complex, 1 μg/ml leupeptin, and 1 μg/ml trypsin inhibitor). The cells were extracted with 0.5% Triton in CSK at 4°C and washed twice with CSK buffer. After washing, cells were fixed in 4% paraformaldehyde in PBS containing 5 mM $MgCl_2$ for 15 min at room temperature. The coverslips were washed twice with, and stored in, 70% ethanol at 4°C.

Ribonuclease Treatment

Paraformaldehyde fixed cells stored in 70% ethanol were rehydrated in 1× PBS containing 5 mM $MgCl_2$ for 10 min at room temperature and rinsed with RNase buffer (10 mM Tris-HCl, pH 7.5, 150 mM NaCl, 1.5 mM $MgCl_2$). The cells were then treated with RNase A (0.2 mg/ml), RNase T_1 (0.2 mg/ml) in RNase buffer for a short time at room temperature. Under this condition the poly(A) region of mRNA is resistant to degradation by ribonuclease (Kish and Pederson, 1976; Kwan and Brawerman, 1972). For control experiments, cells were treated with RNase A (0.2 μg/ml), RNase T_1 (0.2 μg/ml), and RNase T_2 (1,000 U/ml) for 30–60 min at 37°C before hybridization.

Drug Treatment

For experiments requiring the release of ribosomes and protein synthesis inhibitors, cells were treated with puromycin (100 μg/ml), NaF (10 mM), cycloheximide (5 μg/ml), and emetine (50 mM) for 30 min at 37°C and then fixed with paraformaldehyde. Parallel experiments were done by extracting the cell with 0.5% Triton in CSK buffer before fixation. For disrupting the specific filaments, cells were treated with colcemid 5 μg/ml for 1 h to depolymerize the microtubules and for 3 h to collapse the vimentin filaments perinuclearly. The cells were treated with cytochalasin D for 30 min to depolymerise the actin filaments. After drug treatment, the cells were fixed in paraformaldehyde with and without Triton extraction.

Immunofluorescence Labeling

Cells were rinsed with PBS containing 0.1% Triton for 5 min at room temperature and then with PBS for 2 min. In case of actin filaments, cells were incubated in FITC-phalloidin (Molecular Probes, Inc., Eugene, OR) 1:10 diluted in PBS (10 μg/ml) at 37°C for 30 min. After incubation cells were washed twice with PBS for 30 min each, and mounted on the slide in DABCO. For microtubules, actin filaments, and vimentin filament labeling, cells were incubated at 37°C for 30 min either with mouse anti-tubulin (Amersham Corp.) diluted 1:50 in antibody dilution buffer (2× SSC, 2% goat serum, 1% BSA, and 0.05% Triton) or with mouse anti-actin (East-Acres Biologicals, Southbridge, MA) diluted 1:50 in antibody dilution buffer or with mouse anti-vimentin (Amersham Corp.) diluted 1:20 in antibody dilution buffer. Cells were washed with 2× SSC, 0.05% Triton for 30 min at room temperature. After washing, cells were further incubated with FITC-conjugated goat anti-mouse IgG (Cappel Laboratories, Malvern, PA) 1:50 diluted in antibody dilution buffer for 30 min at 37°C. After incubation cells were washed two times with 2× SSC, 0.05% Triton for 30 min each, and once with PBS for 2 min at room temperature. The coverslips were mounted in DABCO.

Membrane Labeling

Paraformaldehyde-fixed cells were washed with 0.1 M sucrose and 0.1 M sodium cacodylate, pH 7.6, for 10 min at room temperature. Cells were stained with 2.0 μg/ml of $DiOC_6$ (3, 3'-dihexyloxacarbocyanine iodide, a lypophilic cationic fluorescence dye selectively stained mitochondria and ER) for 30 s at room temperature (Terasaki et al., 1984). The coverslip was washed with 0.1 M sucrose and 0.1 M sodium cacodylate, pH 7.6, for 10 min and then with PBS for 10 min. The coverslip was mounted on the slide with DABCO and visualized under the microscope using a fluorescein filter.

RNA Fractionation

Equal amount of cells (3 × 10^5) were grown in 60-mm dishes and one dish was used for each time point either with or without puromycin (100 μg/ml). Cells were extracted with 350 μl of Triton X-100 (0.5%) in CSK buffer (0.1 M KCl; 0.3 M sucrose; 5 mM $MgCl_2$; 2 mM EGTA; 10 mM Pipes, pH 6.9; 2 mM Vanadyl complex: 1 μg/ml leupeptin; 1 μg/ml trypsin inhibi-

tor; and 1.2 mM PMSF) for indicated time. The supernatant was collected in a microfuge tube containing 50 μl of 10% SDS. Cells were further extracted with 300 μl of RSB (Ornelles et al. 1986) Majik buffer (1% deoxycholate; 0.5% Tween 40; NaCl 10 mM; $MgCl_2$ 3 mM; Tris 10 mM, pH 7.4; PMSF 1.2 mM; Vanadyl complex 2 mM) with vigorous disruption of cytoskeleton. Nuclei were removed by centrifugation at 5,000 *g* for 5 min and the supernatant was collected in a tube containing 50 μl of 10% SDS. The nuclear pellet was suspended in 300 μl of RSB Majik buffer and 50 μl of 10% SDS, the solution was passed through a small bore three times to shear the nucleus. All the samples were extracted twice with phenol and chloroform and precipitated with 2 1/2 vols of ethanol. The RNA pellet was washed with ethanol and lyophilized. Triton supernatant and wash RNA were combined and the RNA was dissolved in 20 μl of Diethyl pyrocarbonate-treated water. RNA was transferred to slot blot and hybridized with p^{32}-labeled poly dT (55-mer) probe. The blot was quantitated by beta-scan or densitometry.

Digital Imaging Microscopy

Image Acquisition. Images of the distribution of fluorescence in single cells were obtained with a Zeiss IM-35 microscope (Carl Zeiss, Inc., Thornwood, NY) equipped for epifluorescence and modified to obtain images at various planes within the cell (Fay et al., 1989). Changes in position of the focus were effected by a computer-controlled stepper motor using feedback from an eddy current sensor that sensed the position of the nose piece relative to the underside of the specimen stage. Images at each focal plane were acquired with a thermoelectrically cooled CCD (model 220; Photometrics Inc., Tucson, AZ) using an RCA CCD chip whose output was digitized with an accuracy at $1:2^{14}$ at 50 kHz. The duration of exposure of the specimen to the excitation source was by a computer-controlled shutter and wavelength selector system. Camera and microscope functions were controlled and coordinated by a PDP–11/73 microcomputer and data acquired from the CCD was stored on hard disk and subsequently transferred via Ethernet to a Silicon Graphics 4D/GTX super work station for further processing. Data was archived on a Tahiti Erasable Optical Disk having 1 GB capacity. To be able to subsequently process images to remove out-of-focus information the 3-D optical transfer function of the microscope was determined each day by obtaining a series of optical sections of a .19-μm diameter latex sphere in which fluorophors with appropriate emission characteristics were embedded (Molecular Probes, Inc.). Typically, images of the point fluorescence source were obtained at .25-μm intervals and a total of 15 images above and below the point of optimum focus was obtained. In addition, for each experiment we recorded the dark current from the camera and a flat field to correct for nonuniformities in the transmission characteristics of the optics and CCD detector.

Image Restoration. To obtain a more precise view of the distribution of molecules that were fluorescently labeled in individual cells, the series of optical sections taken of each cell was subject to further processing to correct for the distortions introduced by the microscope and camera system. The process used is based upon regularization theory and constrains the solution to the inverse problem to be nonnegative (i.e., regions devoid of fluorescent molecules can have values no less than zero). Basically, the problem is formulated to obtain an estimate of the molecular distribution inside the cell that represents a balance between finding the estimate that represents a least-squares best fit to the data and an estimate which is most smooth as defined by the L^2 norm. The extent to which the solution satisfies one or the other condition is determined by a weighting constant which for these studies was typically set at 10^{-4} representing the extent to which the smoothness criteria was used in the estimation of molecular distribution within the cell. We have previously shown that the images of molecular distribution obtained are relatively insensitive to the weighting constant used for the amount of smoothness used in the restoration algorithm. The algorithm has been described in considerable detail (Fay et al., 1989; Carrington et al., 1990). The estimate of molecular distribution is found using this theory in an interactive manner and typically satisfactory restoration took 50 iterations (further iterations produced no detectable improvement in the clarity within the image).

Visualization and Analysis. Individual optical sections in the restored 3-D data sets were inspected and analyzed using computer graphics software developed for the Silicon Graphics super work station which are now available for a PC from CSPI, Inc. (Billerica, Mass.). To assess the amount of label present in the nucleus and cytoplasm of any cell, individual optical sections were displayed and a mouse-driven cursor used to outline the cell perimeter as well as the perimeter of the nucleus. The computer then calculated the sum of the intensities present within the cytoplasm and nucleus, respectively. The complete 3-D arrangement of molecules in the cell could be visualized by projecting the 3-D data set from different perspectives and then displaying those different perspective views sequentially and using kinetic clues to assess the 3-D relations of fluorescent structures within the cell. Alternatively, two different perspective views of the 3-D data sets separated by 12° were displayed on the odd and even lines of a special video monitor having a Tecktronics Magic Window placed in front of the viewing screen to allow the investigator to simultaneously see with the left and right eye, two different views of the distribution of molecules within a cell. The binocular disparity in those two images provided the necessary cues for the investigator to assess the 3-D relations of molecules within the cell. In cells that were labeled for two different classes of molecules, using two different colored fluorophores we assessed the extent to which the two molecules were similarly distributed by calculating the percent of the fluorescent signal of one molecule that codistributed in 3-D with the other. This could be visualized by combining the two images and coding the information in each of the two image pairs in two different colors (typically red and green) and turning those voxels that contained both labeled molecules at levels above threshold white. Those voxels containing neither molecule were black. The codistribution as a function of threshold levels is described in more detail in the Appendix.

Results

The Distribution of Poly(A) RNA in Single Cells Using Conventional Microscopy

The intracellular distribution of poly(A) RNA was revealed by high resolution fluorescence in situ hybridization using a poly dT probe (55 bases) end-labeled with biotin and detected with fluorescein or Texas red–conjugated avidin. Fig. 1 *A* shows the detection of poly(A) RNA within the nucleus and cytoplasm. No signal was detected when biotinylated poly dA (55 bases) probe was used on the same cells (Fig. 1 *C*), and treatment with RNAses A, T_1, and T_2 before hybridization with biotinylated poly dT (Fig. 1 *D*) confirmed that the signal in Fig. 1 *A* resulted from hybridization to poly(A).

The distribution of poly(A) was nonrandom throughout the cell. Discrete focal concentrations of poly(A) were seen in the nucleus and these observations have been described in more detail elsewhere (Carter et al., 1991). We concentrate here on the mRNA component of poly(A) in the cytoplasm. As could be seen in the phase-contrast micrograph (Fig. 1 *B*), the signal became weaker as the cytoplasm become less phase dense. Patchy areas in the cytoplasm could be seen where little poly(A) could be detected. These darker patches appear to be parts of the internal membrane system, and were verified by the use of the lipophilic, cationic fluorescent dye, $DiOC_6$ (Terasaki et al., 1984) which filled these "holes" in the poly(A) signal. Fig. 1, *E* and *F* shows the distribution of poly(A) compared with the membrane signal. Where poly(A) and membranes overlap, a yellow color is evident. The green represents the holes filled with membrane.

Quantitation of Poly(A) Retention After Drug Treatments and Triton Extraction

The amount of fluorescent probe hybridized to an individual cell was quantitated using digital microscopy. The 2-D projection of each cell was measured (this is a good approximation of volume since the cells were very well spread and flattened to the substrate) and the absolute amount of poly(A) in the nucleus and cytoplasm in each cell compared.

To quantitate the poly(A) content of single cells, we measured the amount of fluorescence obtained from each cell

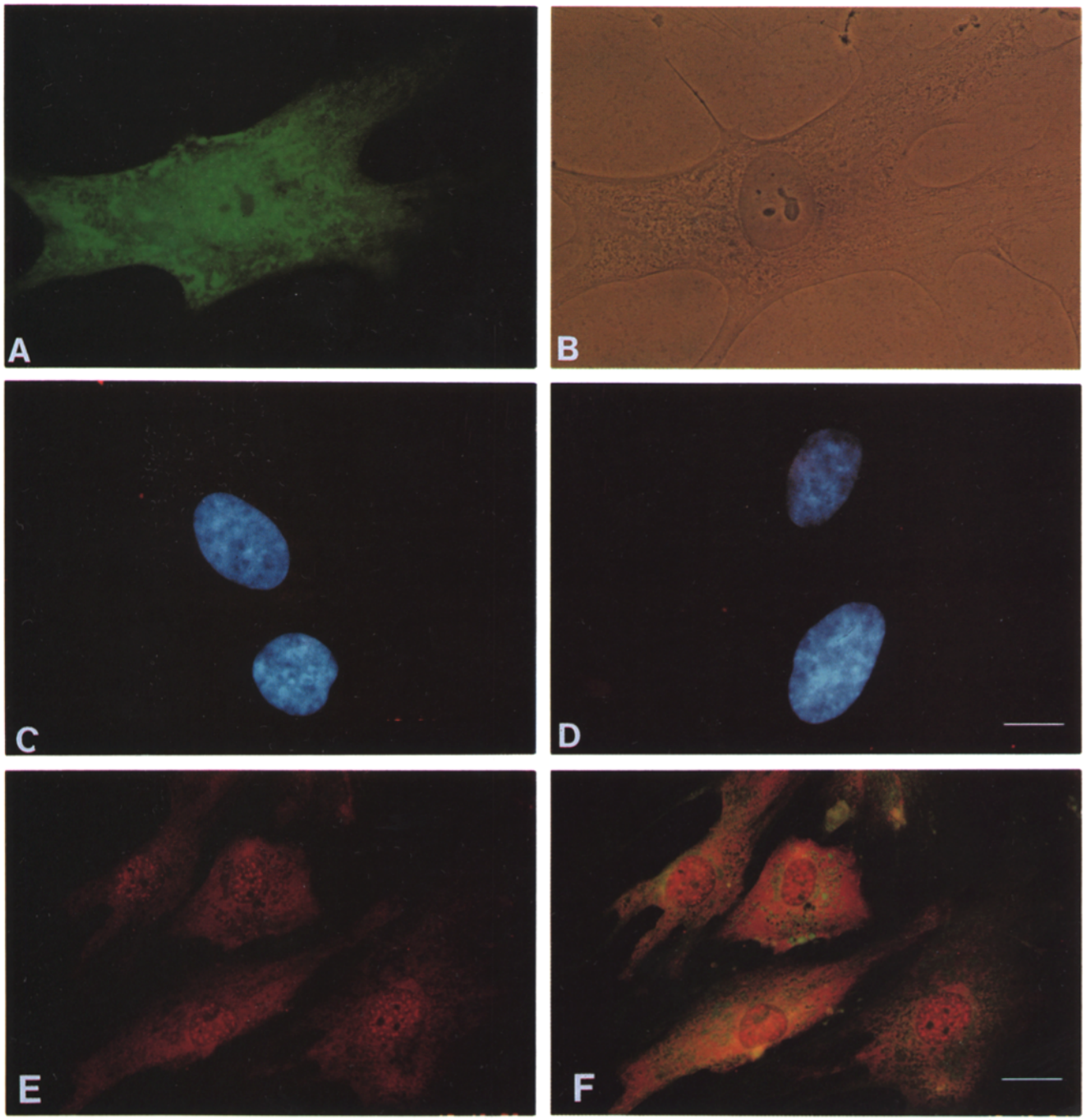

Figure 1. Detection and distribution of poly(A) RNA intracellularly. Human diploid fibroblast cells were fixed and then hybridized with biotinylated oligonucleotide probes and the hybridized probe was detected with avidin conjugated to fluorescein or Texas red. (*A*) Cells hybridized with poly dT-biodUTP probe detected with avidin–fluorescein; (*B*) phase–contrast picture of *A*; (*C*) cells hybridized with poly dA-biodUTP probe detected with avidin and Texas red counterstained with DAPI (double exposure); (*D*) same as *A* but the cells were treated with RNAse A, T_1, and T_2 before hybridization and were also counterstained with DAPI (double exposure); (*E*) same as *A* but detected with Texas red avidin conjugate; and (*F*) cells in *E* were further stained for membranes by lipophilic dye $DiOC_6$. Bars: (*A–D*) 16 μm; (*E* and *F*) 24 μm.

using an interactive computer imaging system. Total fluorescent light was captured and digitized using a cooled, slow scan CCD camera and a PDP11/73 computer (see Materials and Methods) and displayed on a graphics screen. Random cells were chosen, the nucleus and cytoplasm outlined, and numerical values obtained for the total integrated fluorescence intensity (IFI) of each cellular compartment. Measurements of single cells showed a linear relationship using a least-squares fit when comparing cytoplasmic signal with cytoplasmic area (Fig. 2 *A*). This indicated that cytoplasmic concentrations of poly(A) (per unit area) remained mostly constant despite variations in cytoplasmic or nuclear size, or detergent treatment (see below). This suggests that the concentration of poly(A) RNA within each cellular compart-

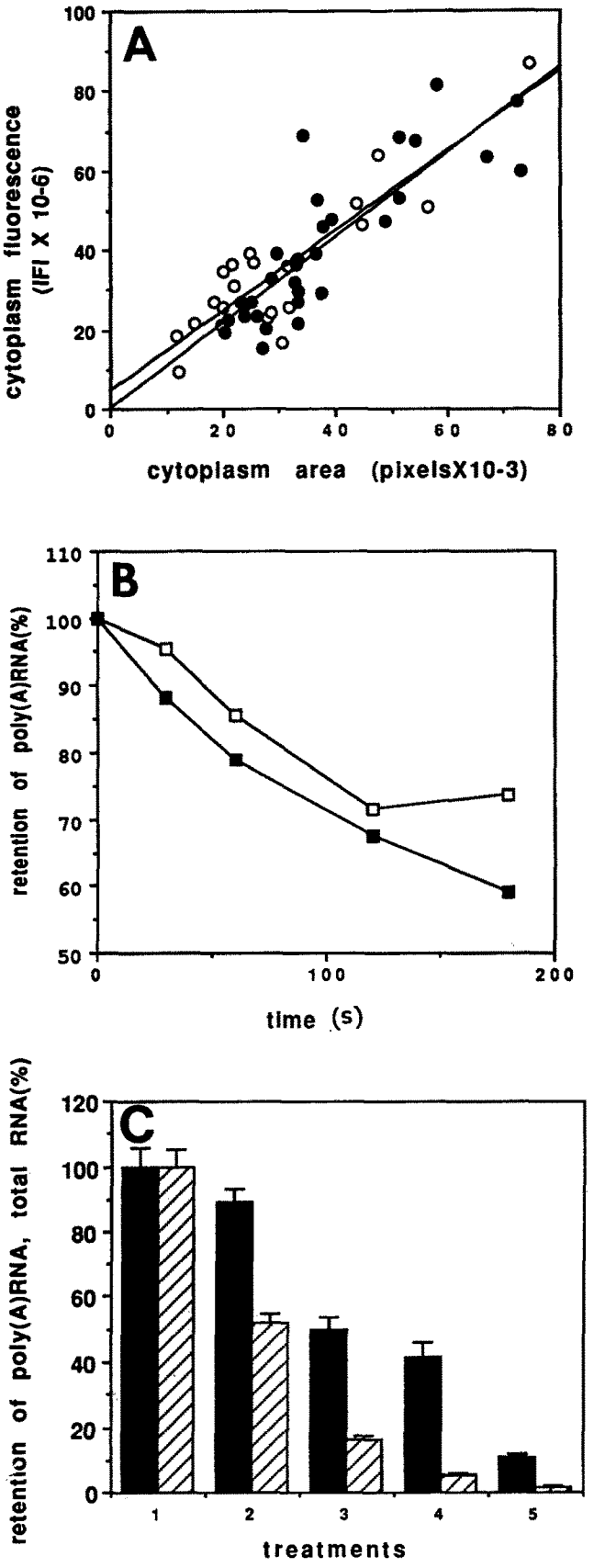

Figure 2. Quantitation of poly(A) and total RNA in cell populations and in single cells (Triton, puromycin, and RNAse treatment). (*A*) Poly(A) content in the cytoplasm of individual cells. Human diploid fibroblasts were hybridized with biotinylated poly dT probe and detected with fluorescein-conjugated avidin. Random cells were chosen from 2–3 coverslips for control and Triton-extracted cells, and the images were taken by CCD camera. The area in pixels (each pixel equals 0.246 μm^2) and the amount of the signal in the nucleus and cytoplasm was isolated on an interactive graphics screen and processed (see Materials and Methods). Data was fit with the least-squares method. Control (○) (n = 22); Triton extraction (●) (n = 30). (*B*) Retention of poly(A) RNA in cell populations: effects of Triton and puromycin treatment. Cells grown on plastic dishes (60 mm, 3 × 10^5 cells) were washed and extracted with Triton. At various times the supernatant was removed and cells were scraped off the plate and separated into nucleus and cytoskeleton. RNA isolated from each fraction was blotted onto a filter, probed with γ-p^{32}ATP labeled-poly dT (55-mer). Radioactivity was detected using a betascope or optical density scanning. Nonsoluble poly(A) (□); nonsoluble poly(A) after treatment with puromycin for 30 min before Triton extraction (■). (*C*) Retention of poly(A) and total RNA in the cytoplasm of single cells: effects of Triton, puromycin, and RNAse. Control cells were treated as described from left to right: (*1*) no treatment (n = 22); (*2*) Triton extracted for 1 min (n = 30); (*3*) puromycin treatment for 30 min before Triton (n = 20); (*4*) RNAse A and T_1 for 5 min at room temperature after Triton and fixation (n = 7); and (*5*) RNAse A, T_1, and T_2 for 30 min at 37°C after Triton and fixation (n = 3). Cells were then subjected to in situ hybridization and the poly(A) RNA detected by avidin fluorescein and the total RNA (mostly ribosomal RNA) in the same cells by propidium iodide. The cells were then analyzed by digital imaging microscopy and an interactive graphics program to measure the total integrated fluorescence intensity from the nucleus and the total cell. The cytoplasm (total cell minus nucleus) was plotted as an average value. The untreated cells were set at 100% and all subsequent measurements expressed as a percent of control. Bar represents SEM. Poly(A) RNA (fluorescein) (■); total RNA (propidium iodide) (▨).

ment is maintained constant by the cell. Biochemical studies have shown that the cell extracted with the nonionic detergent Triton X-100 solubilizes most of the cytosol but leaves the cytoskeletal framework intact (Lenk et al., 1977; Jeffrey, 1984; Pudney and Singer, 1979). To evaluate the association of poly(A) with this cellular structure, we used two means of quantitation. The first was quantitation of in situ hybrids in individual cells, using digital imaging microscopy and the second was a biochemical approach in which cells were fractionated. To visualize the distribution of poly(A) RNA directly on the cytoskeleton of human diploid fibroblast cells, cells were extracted with 0.5% Triton and fixed in paraformaldehyde before hybridization. Statistically, little difference between the absolute amount of poly(A) RNA was detected when comparing the two cell populations.

The retention of poly(A) RNA after extraction in Triton was then analyzed biochemically as a function of time in extraction buffer (Fig. 2 *B*). RNA was extracted from the Triton supernatant and the remainder of the cell. The isolated RNA was adsorbed to filters ("slot blot"), then hybridized with poly dT probe labeled with ^{32}p-γ-ATP, and the amount of hybridization determined directly using quantitation of the radioactivity directly (Betascope 603; Betagen, Waltham, MA) and densitometry. Each fraction was expressed as a percent of total poly(A) RNA in unextracted cells. ~27% of the poly(A) dissociated from the cytoskeleton in the first 3 min of extraction and little change was seen subsequently up to 10 min.

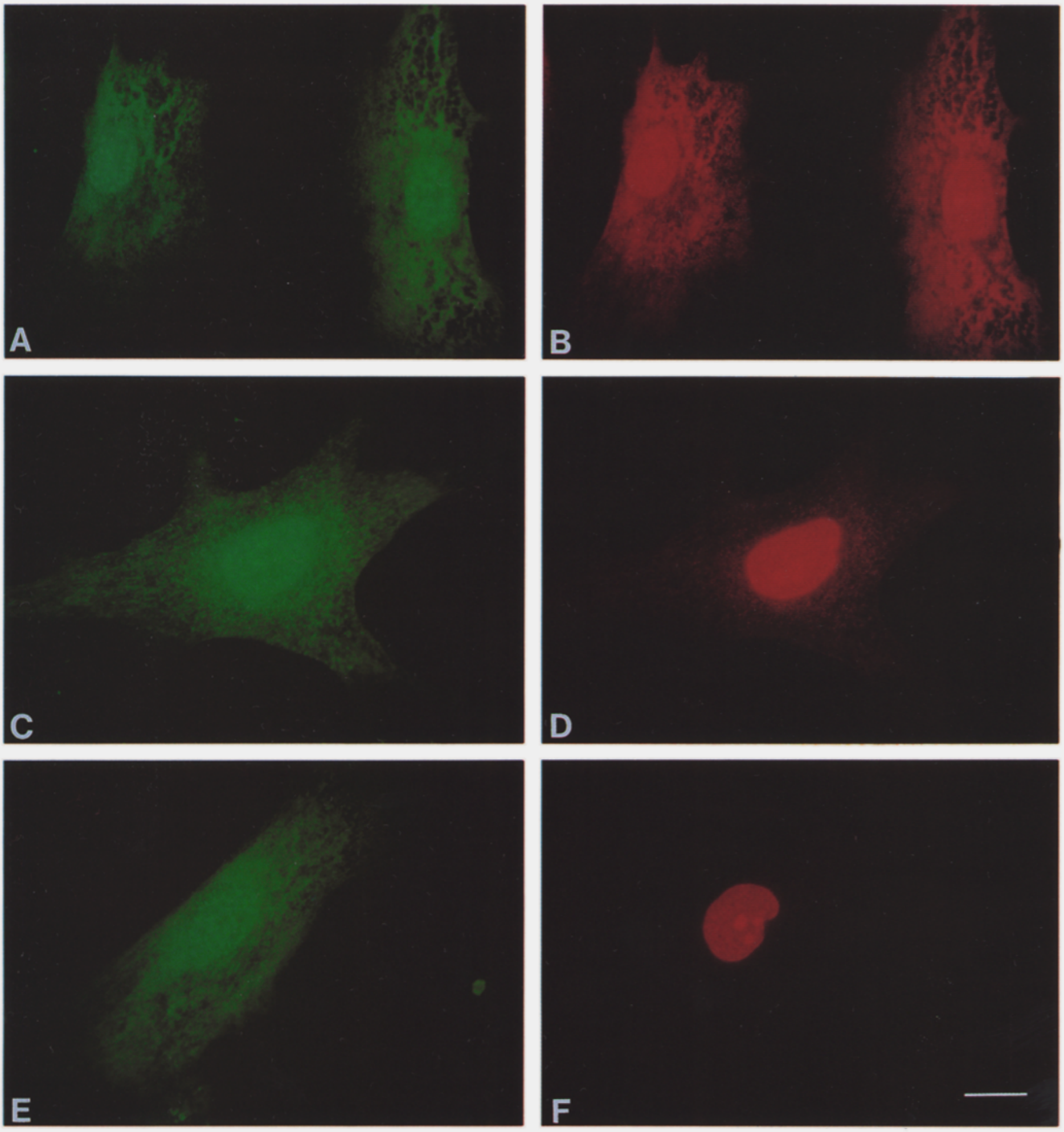

Figure 3. Retention of poly(A) RNA and total RNA visualized in single cells: effect of Triton extraction, puromycin, and RNAse. (*A*, *C*, and *E*) Poly(A) RNA detected in Triton-extracted cells (1 min) using poly dT-biodUTP hybridized and detected with avidin–fluorescein conjugate. (*B*, *D*, and *F*) Total RNA detected in the same cells with propidium iodide (DNA was also detected in the nucleus). (*C* and *D*) Puromycin treatment before Triton extraction and fixation. (*E* and *F*) RNAse A- and T_1-treated cells after Triton extraction and fixation. Exposure times were (*A*, *C*, and *E*) 45 and (*B*, *D*, and *F*) 15 s, both on Kodacolor Gold 400 ASA film (Eastman Kodak Co., Rochester, NY). Bar, 17 μm.

A second fluorescent (red) label, the intercalating dye propidium iodide was used (Frankfurt, 1980) to detect double-stranded RNA most of which is ribosomal RNA. This provided an additional measure of the RNA content (red) independent of poly(A) (green) and also was indicative of the functional state of the mRNA. Polysomes still remained attached to the message through the Triton extraction as indicated by the propidium iodide signal (Fig. 3 *B*). The histogram in Fig. 2 *C* (*2*) represents the percent loss of poly(A) RNA and total RNA (ribosomal RNA) with Triton extraction and represents a summary of Fig. 3, *A* and *B*. Triton extraction for 1 min removed ~11% of the poly(A) sig-

nal, in agreement with results obtained using biochemical fractionation techniques (Fig. 2 *B*). However it removed half of the ribosomal signal suggesting that these represented ribosomes unassociated with mRNA.

The role of ribosomes and nascent polypeptide chains in the association of poly(A) RNA to the cytoskeleton was investigated by treating the cells with puromycin before cells were extracted with Triton and fixed with paraformaldehyde. The visualization of single cells is represented in Fig. 3, *C* and *D* and shows that poly(A) signal can be quantitatively and spatially separated from ribosomal signal. Dissociation of ribosomes and nascent chains from mRNA resulted in >50% of the poly(A) RNA remaining in the cell after in situ hybridization whereas the ribosomal RNA was reduced to <16% after in situ hybridization (Fig. 2 *C*, *3*). This suggests that the remaining mRNA is associated directly with the cytoskeleton, rather than through the ribosomes or nascent chains. This also confirms the use of propidium iodide as a ribosome-specific stain.

The loss of poly(A) RNA after in situ hybridization was ~39% more when cells were treated with puromycin before Triton extraction. When the retention of poly(A) was measured by fractionation of the cell (Fig. 2 *B*), there was a loss of poly(A) RNA ~10–20% more with puromycin in the cytoplasm (we measured nuclear poly(A) RNA to be 19% of cellular poly(A) and this remained unaffected with puromycin). This loss of poly(A) RNA with puromycin treatment may be expected of messages which were attached via nascent chains; there is a possibility that these were membrane-associated messages. The higher retention of poly(A) using fractionation compared with hybridization to single cells may be in part due to the inability of the fixative to retain the poly(A) throughout the rigorous conditions of in situ hybridization. We have shown a loss of actin mRNA from extracted cells when paraformaldehyde was used as a fixative instead of glutaraldehyde (Singer et al., 1989). In this case where fixation in paraformaldehyde was necessary due to induced autofluorescence by glutaraldehyde, the increased loss of in situ hybridization over cell fractionation (~29%) after puromycin treatment followed by 1 min of Triton extraction may reflect the fact that ribosomes or nascent chains provide additional stability by cross-linking poly(A) RNA to the cytoskeleton. To minimize these losses, we developed a less disruptive protocol, using 15% formamide and hybridization for only 1/2 h. This substantially reduced poly(A) loss and supported this interpretation (data not shown).

Since the results with puromycin and Triton extraction indicated that the majority of poly(A) RNA was associated directly with the cytoskeleton, we wished to evaluate in more detail whether poly(A) or some other part of the mRNA molecule was involved in binding this subset of mRNA to the cytoskeleton. The distribution of poly(A) occasionally suggested association with fibrils (Fig. 3 *A*). Cells fixed on coverslips were treated with RNase A and T_1 under conditions which digest the mRNA but to which the poly(A) is resistant (Kish and Pederson, 1976; Kwan and Braverman, 1972). If poly(A) is necessary for binding mRNA to the cytoskeleton, the relatively insensitive poly(A) region should remain attached to the cytoskeleton. However, if poly(A) is not involved in binding the rest of the mRNA to the cytoskeleton, digestion of non-poly(A) regions should release it. The results are shown in Fig. 3, *E* and *F*. When poly(A) RNA was digested with RNase A and T_1 under conditions which protect the poly(A) tail, 42% of the poly(A) remained attached to the Triton-extracted cytoskeleton and the ribosomal RNA revealed by the propidium iodide stain was reduced to background levels (~1.9%) (Fig. 2 *C*, *4*), as would be expected if the mRNAs to which polyribosomes attach is released. The digestion of the mRNA was further confirmed by Triton extracting the cells, treating with low levels of RNase A and T_1, isolating the cytoskeletal bound and released RNA and then blotting the fraction and then probing each fraction for poly(A) or actin mRNA and tubulin mRNA. Both mRNAs were digested from the cytoskeleton but poly(A) remained (Fig. 4). This result suggested that a significant fraction of the poly(A) was attached to the cytoskeleton, either directly or near enough to be fixed onto the filaments during fixation. Since the amount of poly(A) retained in puromycin-treated cells and RNase-treated cells is almost equal, it is possible that this is the same population of poly(A) RNA, and represents molecules which are anchored to the cytoskeleton directly or indirectly through the poly(A) tail. The released molecules may belong to the subset attached via nascent chains, some non-poly(A) part of the RNA, or molecules with weak affinity to the cytoskeleton.

Association of Poly(A) RNA with Actin Filaments

Because in situ hybridization revealed the spatial distribution of poly(A) RNA in single cells for the first time, codistribution with other cellular structures can be investigated. To determine which of the cytoskeletal components is associated with poly(A) RNA, we used fluorescent in situ hybridization coincident with immunofluorescence for specific cytoskeletal filaments in individual cells. Fig. 5, *A*, *C*, and *E* shows the hybridization pattern to poly(A) RNA (red) labeled with antibodies for vimentin, tubulin, and with phalloidin for actin filaments (green), respectively. The detection of actin by phalloidin stains predominantly stress fibers. Where the red and green colors are congruent, a combined yellow color was evident. The double label immunofluorescence demonstrated that none of the fibers visualized by these antibodies showed a complete congruence with the poly(A) signal.

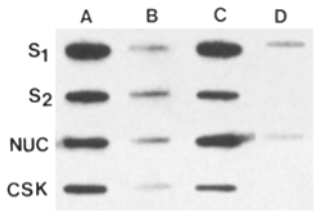

Figure 4. Preferential retention of poly(A) on the cytoskeleton compared to tubulin or actin-mRNAs. Human fibroblasts in culture were extracted with 0.5% Triton in CSK buffer for 1 min, the supernatant was removed, and the pellet was treated with RNAse A and T_1 for 10 min at 4°C. The supernatant was removed and the cells were vortexed and separated into nuclear and cytoskeletal fractions. RNA was isolated from each fraction and blotted onto nitrocellulose papers. One blot was probed with γP^{32}-ATP labeled poly dT (55 bases) and the other was probed with P^{32} nick-translated actin and tubulin cDNA probe. (*A* and *B*) Cells were treated with 0 U of RNAse; (*C* and *D*) cells were treated with 10 U each of RNAse A and T_1; (*A* and *C*) probed with poly dT; and (*B* and *D*) probed with tubulin and actin cDNA. *S_1*, Triton supernatant; *S_2*, RNAse supernatant; *CSK*, cytoskeletal fraction; and *NUC*, nuclear fraction.

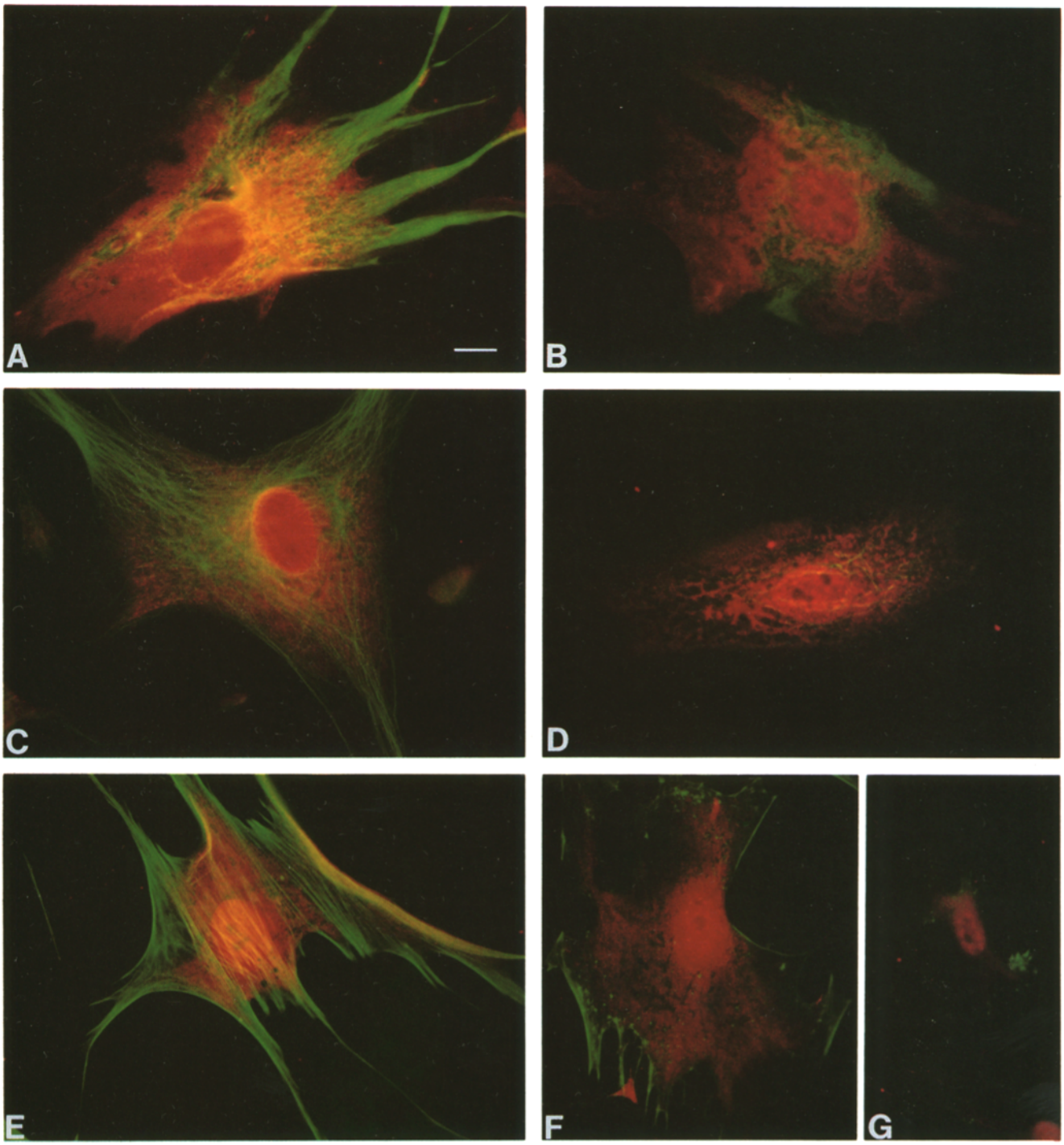

Figure 5. Double labeling of poly(A) RNA and filament proteins in single cells: effect of colcemid or cytochalasin. Poly(A) RNA was detected using avidin–Texas red and cells were then exposed to fluorescein conjugated to phalloidin (actin detection) or antibodies to vimentin or tubulin, cells in *A–D* were double exposures: fluorescein 15 s, and Texas red 45 s. Cells in *E–G* were exposed for 40 s using a dual filter. (*A* and *B*) Poly(A) and vimentin. Colcemid treatment for 3 h in *B* before fixation. (*C* and *D*) Poly(A) and tubulin. *D* was Triton extracted at 4°C (1 min) before fixation. (*E*, *F*, and *G*) Poly(A) and actin. *F* and *G* were treated with cytochalasin D for 30 min before fixation, 0.5 μg/ml and *G* was also extracted with Triton before fixation. Bar, 16 μm.

Therefore poly(A) did not decorate along the length of microtubules, intermediate filaments, or stress fibers. However, it was possible that most of the poly(A) RNA was present on the diffuse network of 6-nm actin filaments, not easily resolved by the immunofluorescence.

If poly(A) was associated with the actin isotopic network, there are three ways to visualize this: to treat the cells with drugs known to disrupt each of the filaments, to use higher spatial resolution light microscopy methods, or to directly visualize the 6-nm filaments by EM. The first two ap-

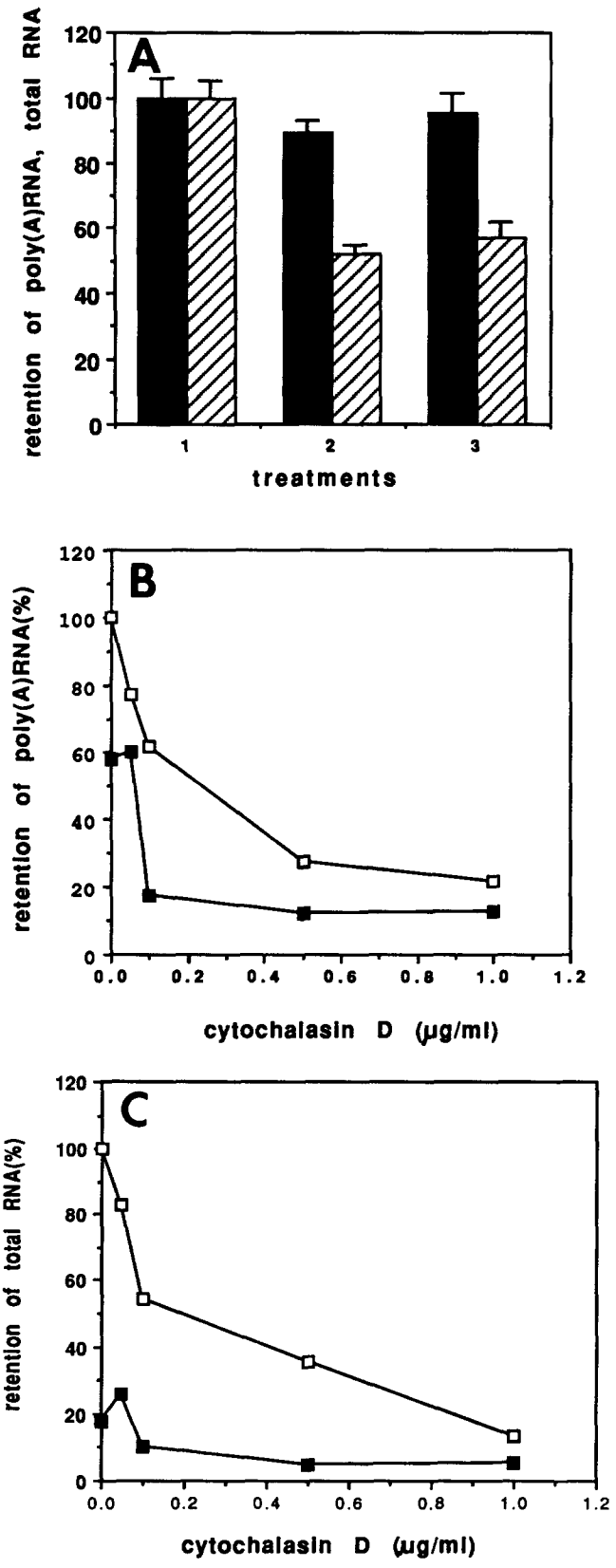

Figure 6. Quantitation of poly(A) and total RNA in single cells after colcemid or cytochalasin D. (*A*) Retention of poly(A) and total RNA in single cells after Triton and colcemid treatment. Cells were treated as follows: (*1*) control cells (n = 22); (*2*) Triton extraction (n = 30); and (*3*) colcemid treatment for 3 h before Triton extraction (n = 10). Cells were then fixed in paraformaldehyde before hybridization with biotinylated poly dT. Quantitation was done by digital imaging microscopy as in Fig. 2 *C*. Poly(A) RNA (fluorescein) (■). Total RNA (propidium iodide) (▨). (*B*) Poly(A) RNA retention in single cells after cytochalasin D treatment, either with or without puromycin. Cells were treated with varying concentrations of cytochalasin D (CD) and then Triton extracted to remove released RNA. Fluorescence in single cells was quantitated by digital imaging microscopy (5–7 cells per point). Signal was expressed as percent of control (Triton-extracted cells with no drug). Poly(A) RNA in Triton-extracted cells exposed to CD (□). Poly(A) RNA in Triton-extracted cells exposed to CD and puromycin (■). (*C*) Total RNA retention in single cells after cytochalasin D treatment. Same samples as *B*, but the total RNA was detected by propidium iodide. Total RNA, Triton, and CD (□). Total RNA, Triton, CD, and puromycin treated (■).

proaches are described here and the ultrastructural approach elsewhere (Bassell, G., C. Powers, K. Taneja, and R. Singer, manuscript submitted for publication). To establish a tighter correlation between poly(A) and particular filaments, we disrupted cytoskeletal filaments and studied this effect on the distribution and retention of poly(A). Because this correlation required more subtle distinctions than an all-or-none effect, it was important to rigorously quantitate the amount of poly(A) affected by each treatment. Triton extraction (Fig. 5 *D*) at 4°C or colcemid (not shown) depolymerized most of the microtubules and after Triton the subunits were released into the supernatant. Neither showed any effect in the retention or the nonrandom distribution of poly(A) RNA. Longer treatments with colcemid (3 h) partially collapsed the vimentin filaments to the perinuclear area, and the retention and more importantly, the distribution of poly(A) was not obviously affected. The spatial partitioning of the vimentin filaments away from part of the poly(A) signal is particularly striking (Fig. 5 *B*). Furthermore, colcemid treatment for 3 h before Triton extraction did not remove significantly more poly(A) RNA or ribosomal RNA than Triton alone showing that most of the poly(A) RNA (~95%) and polysomes (~57%) remained qualitatively (Fig. 5 *B*), and quantitatively (Fig. 6 *A*, *3*) unaffected by these perturbations to microtubules and intermediate filaments. The morphology of the cell was not affected as determined by phase microscopy (Goldman, 1971) and immunostaining by phalloidin showed minimal disruption of actin filaments. This demonstrated that the majority of poly(A) RNA is not linked to the microtubules or vimentin filaments in the steady state, however some overlap with vimentin (yellow areas) is still possible. The association of a subset of poly(A) with vimentin is currently being investigated in detail (Bassell, G., C. Powers, K. Taneja, and R. Singer, manuscript submitted for publication).

In marked contrast, cytochalasin D (Fig. 5, *F* and *G*), which perturbs the actin filament system (Ornelles et al., 1986) caused a drastic effect on poly(A) retention. Untreated cells (Fig. 5 *E*) and cytochalasin D–treated cells (Fig. 5 *F*) show the same distribution of poly(A) even though most of the stress fibers and apparently the actin filaments were disrupted with cytochalasin D (0.5 μg/ml), but some actin filaments still stained with phalloidin along the plasma membrane. However, as soon as the plasma membrane was permeabilized with Triton, a majority of the poly(A)

(~70%) and ribosomal RNA (87%) along with much of the actin protein were extracted into the supernatant (Fig. 5 *G*). This indicated that, after cytochalasin D treatment, this subset of poly(A) RNA was held in place by fixation of the cell, but was no longer attached to cellular structures. The distribution of vimentin filaments was not affected by cytochalasin D and Triton treatment (not shown). Possibly the poly(A) not released by cytochalasin and Triton is retained on the intermediate filament network. This conclusion is supported by quantitative analysis of the fluorescent images obtained under these different conditions. In Fig. 6 *A*, the retention of poly(A) and ribosomes after colcemid and Triton treatment (*3*) showed no significant difference when compared with Triton alone (*2*). Fig. 6 *B* represents the percent retention of poly(A) RNA in the cytoplasm after increasing doses of cytochalasin D with or without puromycin treatment and then subsequent Triton extraction before fixation. Total fluorescence was calibrated on each cell by digital imaging as described in Materials and Methods. In Fig. 6 *B*, 40% of the poly(A) RNA was lost with puromycin treatment alone. An additional 40% loss of poly(A) RNA occurred with very low doses of cytochalasin D (0.1 μg/ml) whether or not cells had been treated with puromycin. This observation suggests that puromycin and cytochalasin may interact with different subsets of poly(A) RNA. Polyribosomes were also quantitated using propidium iodide in the same samples and the signal was released by cytochalasin D identical to the poly(A) (Fig. 6 *C*).

As described previously, the association of poly(A) may be with the single, 6-nm actin filaments. When actin was labeled with FITC-phalloidin, the stress fibers and actin bundles were labeled overwhelmingly and actin meshwork was difficult to visualize (Fig. 5 *E*). To improve the labeling of the meshwork, we screened for and selected a monoclonal actin-antibody (East-Acres Biologicals) which predominantly labeled the actin meshwork rather than the fiber bundles. This antibody was confirmed by Western blots to be specific for actin protein. Previous work (Hoock et al., 1991) has shown that specific mAbs may not decorate stress fibers. This may be due to unavailability of this epitope in the stress fiber. Fig. 7, *A* and *B* shows the correlation of actin and poly(A) in the intact cell. The actin at the leading edge is evident with some poly(A) signal in the lamellipod. We used a Triton-extracted cell to remove G-actin which obscured correlation of F-actin with poly(A) (Fig. 7, *C* and *D*). This showed the spatial distribution of poly(A) RNA (Fig. 7 *C*)

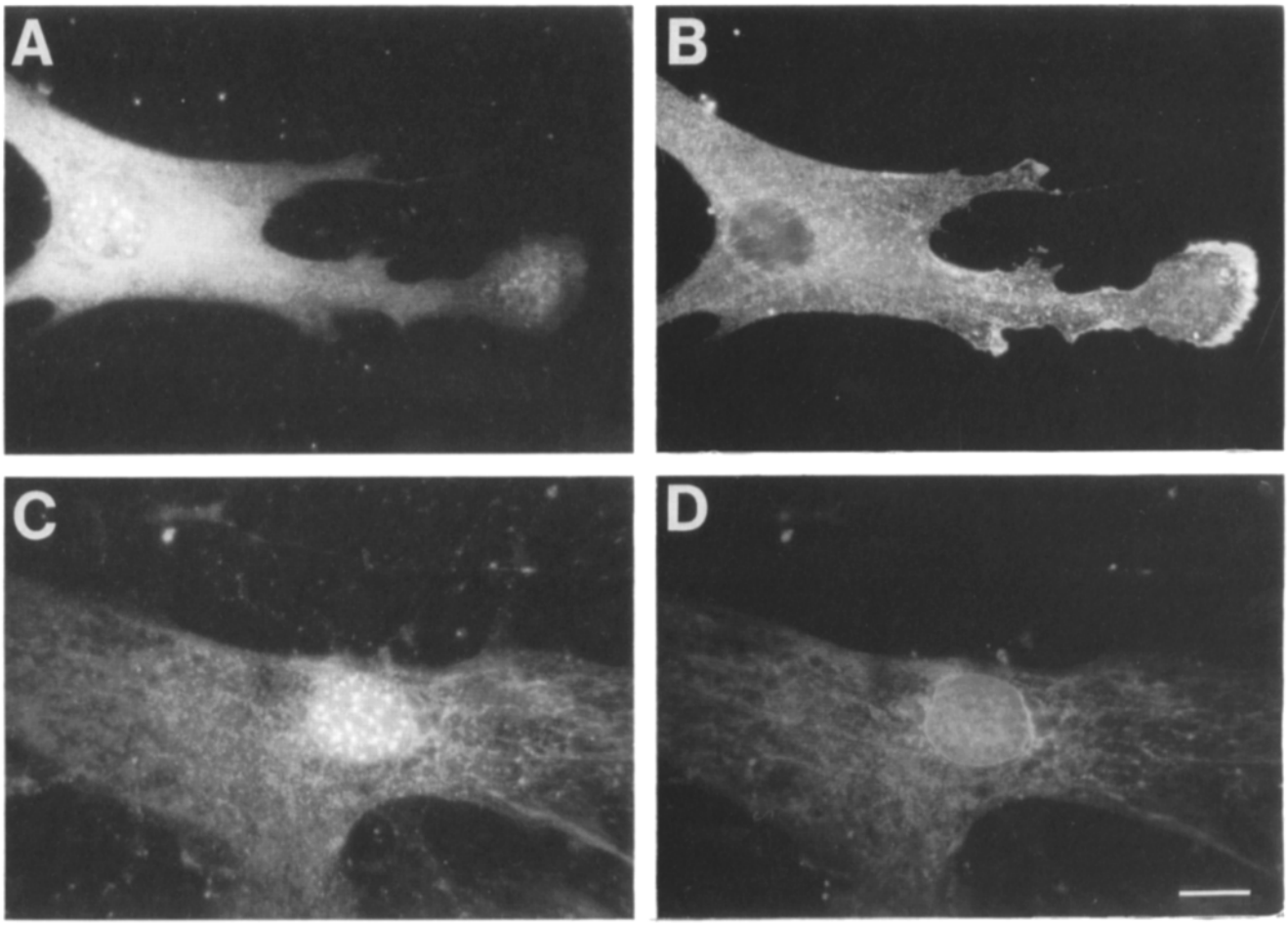

Figure 7. Double labeling of poly(A) and F-actin. Poly(A) was detected with Texas red–conjugated avidin and F-actin detected with an actin-antibody (East Acres Biologicals, Southbridge, MA). Exposure time, 45 s on Kodak TMAX 400 ASA film (Eastman Kodak Co.). (*A*) Distribution of poly(A) in an intact cell; (*B*) distribution of actin as in *A*; (*C*) distribution of poly(A) in a cell extracted with Triton before hybridization; and (*D*) distribution of actin as in *C*. Bar, 16.5 μm.

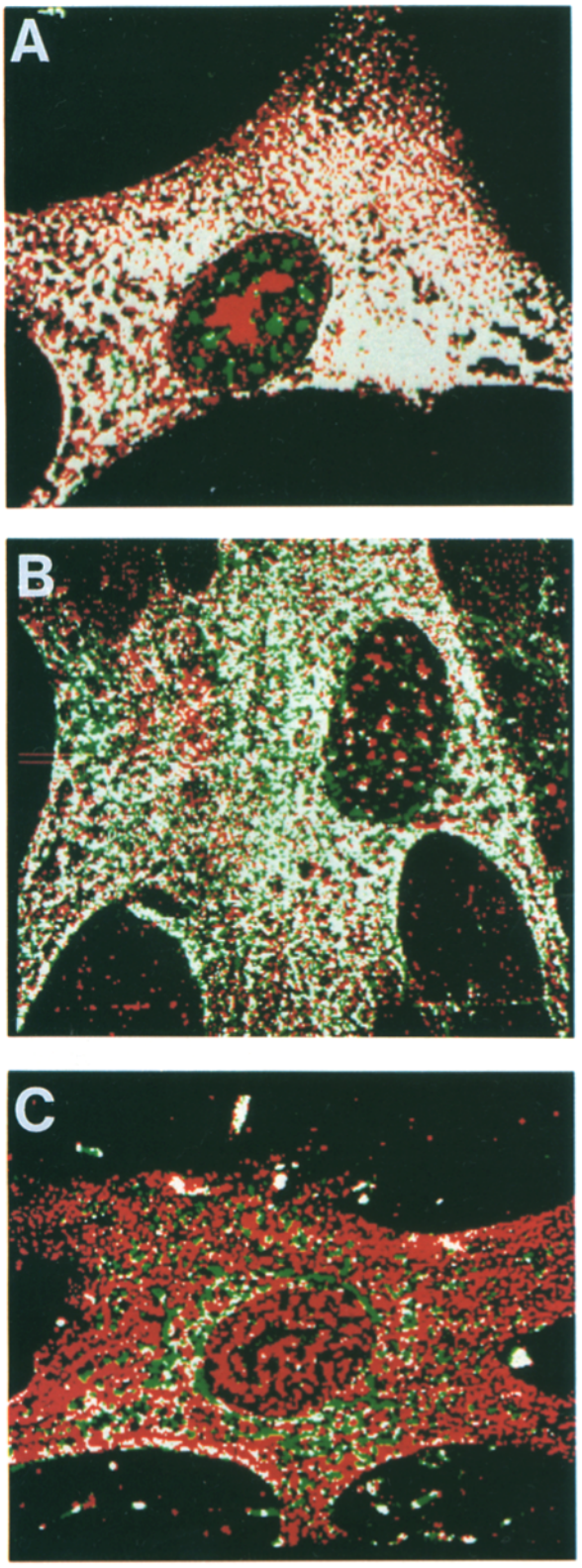

Figure 8. Digital imaging microscopy analysis of the coincidence of poly(A) with ribosomes, membranes, and F-actin. Poly(A) was detected by fluorescein (*A*) or Texas red–conjugated avidin (*B* and *C*) and the cells stained for ribosomal RNA with propidium iodide (*A*), F-actin with actin-antibody (*B*), or for ER with DiOC6 (*C*). Cells in *A* and *B* are Triton extracted. 3-D images were obtained at 0.25 μm intervals in the Z-axis and restored to remove out-of-focus information. After restoration two images at each wavelength (green and red) were taken from the same Z plane and were superimposed. Each image was thresholded above the noise and each pixel which contains both wavelengths is represented as white.

corresponded roughly but not identically with actin filaments (Fig. 7 *D*). In Fig. 7 *D*, actin was detected in the nucleus when the nuclear membrane was permeabilized with Triton, showing some overlap with nuclear poly(A). There was also F-actin associated with the nuclear envelope, only seen after Triton treatment.

To visualize the extent to which F-actin and poly(A) codistribute within the cell, we used the digital imaging microscope to provide an assessment of spatial congruence of the two labels. Optical sections at each wavelength were taken and processed to remove fluorescent light not contributing to the particular section (Fay et al., 1989). Two images from the same plane were then superimposed using fiduciary markers. To facilitate visualization of the codistribution, we have used the following pseudocoloring scheme: those voxels which contained poly(A) alone were turned red, those that contained only actin were green, those that contained both were white, and those that contained neither poly(A) nor actin were black. Images encoded in the same way were also created for cells dual labeled for one group of poly(A) (green) and ribosomal RNA (red), and another group of poly(A) (red) and membranes (green). These two types of images were obtained to determine the range over which the distribution function varied in these cells: poly(A) and ribosomes would be expected to codistribute closely whereas poly(A) and membranes would not. Fig. 8 shows typical optical sections of cells labeled and displayed in this manner. As expected, the cell labeled for poly(A) and ribosomal RNA has few red and green voxels; most voxels are white or black indicating a high degree of similarity in the distribution of these species (Fig. 8 *A*). In contrast, the cell labeled for membranes and poly(A) (Fig. 8 *C*) has few white voxels and many red and green voxels indicative of a low extent of codistribution of these species. As shown in Fig. 8 *B*, actin and poly(A) appear to have a high degree of codistribution; there are more red and green voxels than the poly(A) ribosome sample but the majority are white. This confirms the high level of codistribution between actin and poly(A). However, when two signals are broadly distributed throughout the cell, it becomes essential to evaluate the degree of colocalization of the two images in an objective manner, to assure that their overlap does not occur solely by chance. A mathematical analysis was therefore undertaken (see Appendix) to determine quantitatively the codistribution of two probes detected by different fluorochromes. This serves as a paradigm for analysis of data obtained by digital imaging microscopy. The images over a range of biologically plausible threshold windows (see Fig. A1) were analyzed for each image pair to determine the probability that the observed codistribution could have been produced by random (i.e., independent) factors (see Figs. A2–A4). None of the image pairs was found to represent independent distributions with respect to each other. That is, the signals of each image were dependent on some cellular feature in common to both. The mean colocalization values for each image pair (determined over a reasonable threshold range) varied between each of the image sets: the poly(A)/ribosome set (Fig. 8 *A*), had 81%

mean colocalization between the two images, the poly(A)/actin pair (Fig. 8 *B*) had 54%, the poly(A) membrane pair (Fig. 8 *C*) had 5.8% (see Appendix for derivations). Therefore this statistical analysis not only provides a quantitative approach to digital image colocalization, but also confirms visual inspection of codistribution of much of the poly(A) with F-actin. It should be noted that after Triton extraction, the colocalization of poly(A) with actin is 67% of the colocalization of poly(A) with ribosomes, a number that compares favorably with the actual measurements of the proportion of poly(A) associated with actin filaments after cytochalasin treatment.

Discussion

This work defines the spatial compartmentalization of poly(A) RNA within the cytoplasm of the cell and some aspects of the mechanism by which the cell achieves this nonrandom distribution. Considerable previous literature has dealt with the interaction of mRNA, or poly(A) with the cytoskeleton (Lenk et al., 1977; Lenk and Penman, 1979; Cervera et al., 1981; van Venrooij et al., 1981; Jeffrey, 1982; Pramanik et al., 1986; Davis et al., 1987). We extend this work to focus on spatial congruence of nucleic acids with structures or compartments within single cells, and measure the amount and concentration of nucleic acids coincident with other components throughout the cell. This has allowed a view of mRNA–cytoskeletal interactions which involves spatial quantitation.

If mRNA is restricted to a specific cytoskeletal compartment within the cell, the synthesis of proteins must also be subject to these same spatial constraints. This observation would have profound implications for the control of cellular structure and function; roughly two thirds of the mRNA is associated with the actin filament system and therefore there must be a correspondence between the site of protein synthesis and the distribution of actin. Since a complete analysis of the mechanism of protein sorting must include the knowledge as to where proteins begin their journey, this spatial understanding is essential. This becomes even more important when considering that diffusion is severely limited within the cytoplasm (Luby-Phelps et al., 1986). Macromolecules diffuse considerably more slowly than in an aqueous environment and complexes of these macromolecules exceeding 260 Å are immobile (Luby-Phelps and Taylor, 1988). Therefore, the closer a protein can be synthesized to its end site results in promotion of its assembly into multipolypeptide complexes since the site of synthesis can create high concentrations in that region with the minimum diffusion distance. We have already demonstrated that specific messages can be distributed regionally within the cell (Lawrence and Singer, 1986; Sundell and Singer, 1990, 1991) and therefore a mechanism which serves to anchor messages so as to prevent their diffusion would play an important role in the localization of specific sequences. The codistribution of much of the poly(A) with actin filaments detectable at the resolution of the light microscope suggests a physical interaction (within .2 μm). This interaction is corroborated by the resistance of poly(A) to removal from the actin cytoskeleton upon RNase digestion, indicating that poly(A), or sequences very close to poly(A), are involved in this linkage. Possibly the poly(A) binding protein (Sachs et al., 1986) plays some role in this association. Messenger RNA is known to be translated when associated with the cytoskeleton (Cervera et al., 1981) and this translatability can be disrupted by cytochalasin D (Ornelles et al., 1986). The poly(A) binding protein in yeast is important for translation of mRNA, possibly by virtue of its interaction with the 60 S subunit-initiation complex (Sachs and Davis, 1989; Munroe and Jacobson, 1990). Recently, translation initiation has been shown to require a poly(A) binding protein–associated ribonuclease (Sachs and Deardoff, 1992). Furthermore, the elongation factor EFla has been shown to be an actin-binding protein in Dictyostelium (Yang et al., 1990). This evidence points toward an actin associated translation factor interacting with poly(A) which is important for mRNA translation.

While this work addresses the anchoring of mRNA in the steady state, it also has implications for the movement of mRNA through the cell. We have suggested that mRNA (in the case of expression of an integrated EBV genome) follows a "track" from the site of transcription toward the nuclear envelope (Lawrence et al., 1989). This would imply that mRNA can exit asymmetrically into the cytoplasm. If mRNA then becomes loaded with ribosomes, it will be nondiffusible (Luby-Phelps and Taylor, 1988), and hence pile up at the outer nuclear envelope. Therefore a way to move mRNA throughout the cytoplasm must exist. This is another potential role for the microfilament system, and implies that actin-based motility may have a role in this movement. Alternatively, mRNA may diffuse freely to the actin compartment in a receptor–ligand model. This diffusion would occur from the point of nuclear pore exit, and would predict that at this point, the mRNA would be lost upon Triton extraction. However, there is no visible evidence that such a clear zone exists around the nucleus where mRNA can be selectively removed; to the contrary, message appears even more intense perinuclearly.

Actin mRNA in spreading cells can relocalize to the lamellipodia of the cell using primarily actin filaments (Sundell and Singer, 1991). It is not apparent how this mRNA can distinguish different compartments within the same filament system. Possibly this spatial specificity involves proteins which recognize both the nucleic acid and the actin cytoskeleton. The plethora of actin-binding proteins, some of which are involved in motility may help to provide message "flow," and may distinguish subcompartments on the filament system. Finally, while a majority of mRNAs are associated with the microfilament compartment, this work should not de-emphasize the importance of the association of mRNA with other filament systems such as intermediate filaments or microtubules in achieving spatial compartmentalization. The precise evaluation of poly(A)–cytoskeletal interactions will require a high resolution ultrastructural analysis combining in situ hybridization with immunocytochemistry (Bassell, G., C. Powers, K. Taneja, and R. Singer, manuscript submitted for publication).

Appendix: Quantitative Evaluation of the Extent of Colocalization between Two Images

Overview of Statistical Analysis

Two registered images will be completely colocalized if the

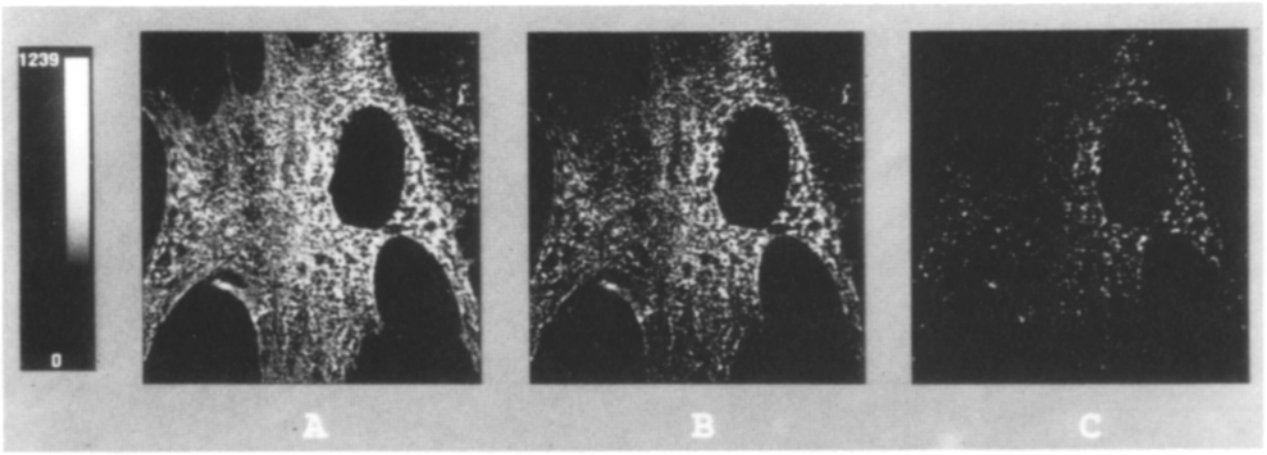

Figure A1. The images from Fig. 8 *B* poly(A) at three different thresholds: (*A*) at a threshold which is too low. The complete filling in of the cell to the very edges is nonbiological for the poly (A) distribution, (*B*) at a threshold with the reasonable range, and (*C*) at a threshold which is too high. Signal is clearly disappearing at threshold in *C* since the poly(A) distributes more completely throughout the cytoplasm (see Fig. A3).

corresponding voxels in each image have equivalent (binary) values. For sparsely labeled images with discrete structures, the nonrandom nature of a high degree of colocalization becomes immediately apparent, e.g., as a visually recognizable pattern. However, when dealing with diffusely labeled structures, it is difficult to determine visually whether the observed colocalization could be due merely to random factors. For instance, since actin and poly(A) are diffusely dispersed throughout the cytoplasm it is important to assess how much of their colocalization could have occurred by chance.

To have confidence in the colocalization numbers produced from the data, two tests must be performed. The first examines the sensitivity of the colocalization to different thresholds which may be used to distinguish signal from background. The second is a determination of the probability that the resulting observed amount of colocalization could have occurred entirely by chance; expressed as the significance that the observed colocalization over the threshold range is due to nonrandom factors (such as intracellular organization). The proportion of the image which is colocalized is less important than whether the observed colocalization (whatever its percentage happens to be) is due to chance or not.

The necessity for examining the sensitivity of the colocalization to thresholding arises because the thresholds used to distinguish signal from background are difficult to precisely define with any degree of certainty. We have chosen to examine colocalization over a range of "reasonable" thresholds for both images involved. Reasonable is defined so that the lowest threshold is clearly too low (some "background" is still seen) and the highest threshold is clearly too high (some specific signal is lost); this threshold range will therefore include the best threshold. For example, Fig. A1 shows the rhodamine-labeled data set of Fig. 8 *B* (the poly[A] actin set) at three different thresholds.

Fig. A3 shows colocalization as a function of thresholds in the fluorescein (abscissa)- and rhodamine (ordinate)-labeled data set of Fig. 8 *B*. The intensity is proportional to the percent colocalization. The range of reasonable thresholds is outlined by a black-white-black border. Within this region the percent colocalization varies from 18–86% of the positive voxels. The colocalization calculated is the probabil-

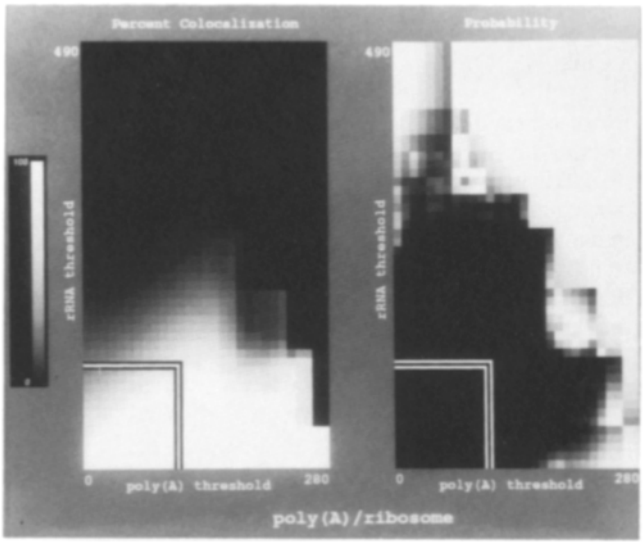

Figure A2. (*Left panel*) Colocalization as a function of thresholds in fluorescein (poly[A]) and propidium iodide (rRNA) in the data set from Fig. 8 *A*. The intensity is proportional to the percent of colocalization. The range of reasonable thresholds is outlined by a black-white-black border. Within this region colocalization varies from 29 to 99%. The mean colocalization is 81% with a standard deviation of 19.6. Note: this colocalization is the probability of observing a rRNA voxel above threshold given that the same voxel in the poly(A) image is above its threshold (see text). (*Right panel*) This image shows the probability that each of the colocalizations (or, more precisely, the observed joint distributions, see the text) shown on the left image could have been generated by independent processes in the two images. Intensity is proportional to probability with white being equal to a probability of one. All probabilities within the reasonable range are essentially zero indicating that the probability of the corresponding voxel in the original images being colocalized randomly is zero. These probabilities were derived by applying a chi-squared test to a contingency table (see text).

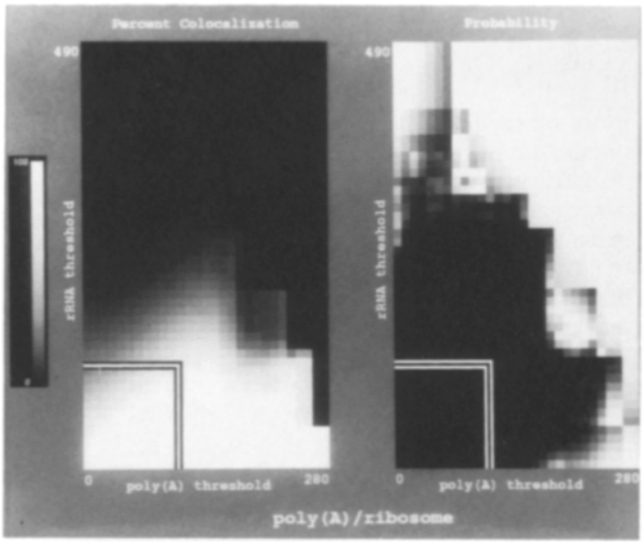

Figure A3. (*Left panel*) Colocalization as a function of thresholds for the data set in Fig. *8 B*. Colocalization varies from 18 to 86% within the specified threshold range. The mean colocalization is 54.0% and the standard deviation is 21.0. Note: this is the probability of observing the actin labeled image given information about the poly(A) image. (*Right panel*) The probability of observing the colocalizations shown on the left if the images were independent. All probabilities within the specified threshold range are zero, i.e., the image sets are not independent (see legend to Fig. A2).

ity of observing a rhodamine-labeled poly(A) voxel above threshold given that the same voxel in the fluorescein (actin) image is above its threshold. In other words, the above threshold voxels in the fluorescein image can be thought of as holes in a mask. The percent colocalization is then the percentage of holes which peer through to an above threshold voxel in the rhodamine image. If the reverse were calculated (i.e., the probability of observing an above threshold fluorescein voxel given that the rhodamine voxel was above threshold) different colocalization percentages would result (but such a calculation would not test the biological question of poly[A] colocalized with actin but rather the less interesting actin colocalized with poly[A]).

Perhaps more important than the exact colocalization percentages is the probability that any of these percentages could have been generated due to random factors. The probability of such an occurrence, for the entire range of reasonable thresholds for the data set in Fig. 8 *B* is essentially zero (see the right image in Fig. A3). These probabilities were derived by applying a chi-squared test to a contingency table (Mendenhall, W. and R. L. Scheaffer. 1973. Mathematical Statistics with Applications. Duxbury Press, North Scituate, MA) as described below. Similarly, Figs. A2 and A4 show colocalization as a function of thresholds and associated probabilities for the data sets shown in Fig. 8, *A* and *C*.

Analysis of a Contingency Table via a Chi-squared Test

The hypothesis that the observed colocalization is due to "random factors" is modeled mathematically by specifying that the probability of voxel i in one image ($V1_i$) being above (or below) threshold T1 is independent of the similarly positioned voxel in the other image being above (or below) its threshold. If this is the case, then $P(V1_i > T1, V2_i > T2) = P(V1_i > T1) * P(V2_i > T2)$. Similarly for the other three possible paired outcomes (e.g., $V1_i > T1$ when $V2_i \leqslant T2$). In other words, the joint probability of a given voxel in image 1 and the equivalent voxel in image 2 both being above (or below) their respective thresholds is simply the product of the individual probabilities [$P(x,y) = P(x)P(y)$]. If the two images are independent of each other, then this relationship will hold (but the converse is not necessarily true). The joint probability of both voxels being above threshold is the probability of a "colocalization event."

To compare the observed joint distribution with the distribution which would be expected if the images were independent of each other, a contingency table (see Fig. A5) is

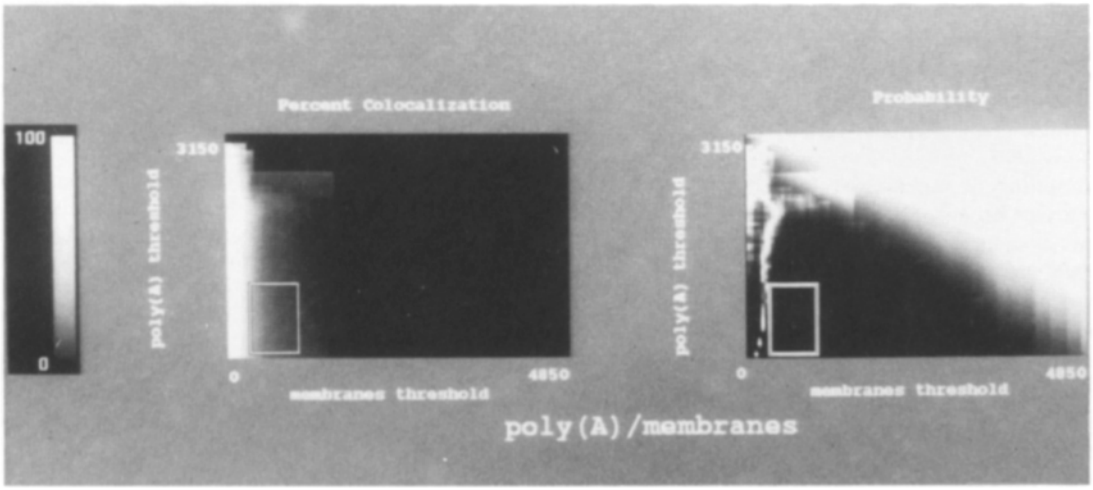

Figure A4. (*Left panel*) Colocalization as a function of thresholds for the data set of Fig. *8 C*. Colocalization varies from 1 to 14% within the specified threshold range. The mean colocalization is 5.8% and the standard deviation is 3.4. Note: this is the probability of observing the membrane image given information about the poly(A) image. (*Right panel*) The probability of observing the colocalizations shown on the left if the images were independent. All probabilities within the specified threshold range are zero, i.e., the images are not independent (see legend to Fig. A2).

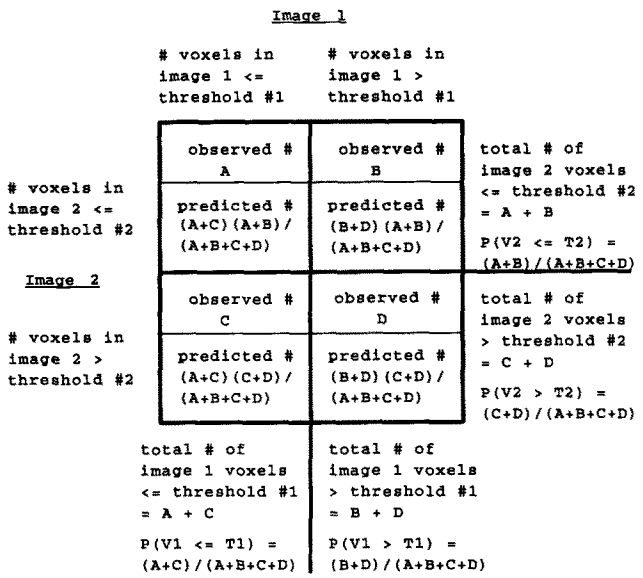

Figure A5. Contingency table for the test of independence of two images.

created and a chi-square test is applied to it. *A*, *B*, *C*, and *D* are the observed number of voxels in each of the four categories. Only voxels in the region of interest of the cell are included (e.g., only those within the cytoplasm, excluding the nucleus). Adding the observations along a row or column and then dividing by the total number of voxels (in the region of interest) produces an estimate of the marginal probability distribution for each image (i.e., the probability of a voxel being above or below threshold given no information about the status of the voxel in the other image). These calculated marginal distributions are the maximum likelihood estimates of the true marginal distributions. Multiplying appropriate marginal probabilities then produces the joint probability of colocalization, assuming independence. This joint probability is then multiplied by the total number of voxels (A+B+C+D) to produce a predicted number of voxels for each of the four colocalization categories. The chi-square test computes the chi-square statistic:

$$X^2 = \sum_{i=1}^{4} \frac{(O_i - E_i)^2}{E_i}$$

This statistic is converted into a probability by calculating the area under a chi-square distribution of one degree of freedom from this value to infinity (i.e., the area of the tail of the distribution). The calculated area is the probability that two independent images would produce an observed distribution which differed by the observed amount or more from the predicted distribution. These are the numbers shown on the right panels of Figs. A2, A3, and A4.

The resulting probability can be used to decide whether the spatial distributions of fluorescence in the two images are independent of each other. For example, if the probability is <.01 it can be concluded that, within a 99% confidence limit, the two image intensity distributions are not independent (i.e., they are dependent). On the other hand, if the probability were equal to, e.g., .2, one could not conclude (at a 99% confidence level) that the images were dependent. It is important to note that in this situation the converse (i.e., that the images are independent) can not necessarily be concluded either. So, if the chi-square statistic produces a very small probability one can confidently state that the images are not independent, but if the probability is "large" it is difficult to conclude anything.

Discussion of the Chi-squared Contingency Table Analysis

This measure of the probability of colocalization due to chance (i.e., due to independent events) has the nice characteristic of being simple to calculate. It also has the important property that it is applicable no matter what the correlation is among pixels within an image. This is necessary since pixel fluorescence is often highly correlated within an image since it is not uncommon for labeled structures to have a spatial extent greater than a voxel (which is typically ~.25 μm in our imaging configuration). The principal limitation of the chi-square test applied to a contingency table, is that it does not include a model of the expected structure shapes and their positions in the images. It is therefore only able to decide dependency when observations produce a small probability and it is not able to decide independence when observations produce a large probability. We are planning on removing this restriction by developing and incorporating models of the expected structures.

Dr. Cindi Sundell provided essential data on the actin antibodies as well as many helpful contributions. Gary Bassell provided correlative data by EM vital to this work. The authors thank E. Fey for the human diploid fibroblasts, D. Bowman for work on imaging microscopy, Walter Carrington for help with algorithms and Jeanne Lawrence and Ken Carter for their helpful discussions.

This work was supported by National Institutes of Health grant HD18066 and National Science Foundation grant BIR 9200027 to F. S. Fay.

Received for publication 17 March 1992 and in revised form 10 July 1992.

Qualitative aspects of poly(A) distribution with the cell were presented at the American Society of Cell Biology meetings (Taneja, K., J. Lawrence, and R. Singer. 1989. *J. Cell Biol.* 109:269a).

References

Adams, A., E. G. Fey, S. F. Pike, C. J. Taylorson, H. A. White, and B. R. Rabin. 1983. Preparation and properties of a complex from rat liver of polyribosomes with components of the cytoskeleton. *Biochem. J.* 216:215–226.

Brawerman, G. 1981. The role of the poly(A) sequence in mammalian messenger RNA. *CRC Crit. Rev. Biochem.* 10:1–38.

Carrington, W. A., K. E. Fogarty, and F. S. Fay. 1990. 3D fluorescence imaging of single cells using image restoration. *In* Noninvasive Techniques in Cell Biology. K. Foskett and S. Grinstein, editors. Wiley-Liss Inc., New York. 53–72.

Carter, K. C., K. L. Taneja, and J. B. Lawrence. 1991. Discrete nuclear domains of poly(A) RNA and their relationship to the functional organization of the nucleus. *J. Cell Biol.* 115:1191–1202.

Cervera,M., G. Dreyfuss, and S. Penman. 1981. Messenger RNA is translated when associated with the cytoskeletal framework in normal and VSV-infected HeLa cells. *Cell.* 23:113–120.

Cleveland, D. W., M. A. Lopata, R. J. MacDonald, N. J. Cowan, W. J. Rutter, and M. W. Kirschner. 1980. Number and evolutionary conservation of α- and β-tubulin and cytoplasmic β- and γ- actin genes using specific cloned cDNA probes. *Cell.* 20:95–105.

Davis, L., G. A. Banker, and O. Steward. 1987. Selective dendritic transport of RNA in hippocampal neurons in culture. *Nature (Lond.).* 330:477–479.

Fay, F. S., W. Carrington, and K. E. Fogarty. 1989. Three-dimensional molecular distribution in single cells analyzed using the digital imaging microscope. *J. Microsc. (Oxf.).* 153:133–149.

Frankfurt, O. S. 1980. Flow cytometric analysis of double-stranded RNA content distributions. *J. Histochem. Cytochem.* 28:663–669.

Goldman, R. D. 1971. The role of three cytoplasmic fibers in BHK-21 cell motility. *J. Cell Biol.* 51:752–762.

Hesketh, J. E., and I.F. Pryme. 1991. Interaction between mRNA, ribosomes

and the cytoskeleton. *Biochem. J.* 277:1–10.
Hoock, T. C., P. M. Newcomb, and I. M. Herman. 1991. B-actin and its mRNA are localized at the plasma membrane and the regions of moving cytoplasm during the cellular response to injury. *J. Cell Biol.* 112:653–664.
Howe, J. G., and J. W. B. Hershey. 1984. Translational initiation factor and ribosome association with the cytoskeletal framework fraction from HeLa cells. *Cell.* 37:85–93.
Isaacs, W. B., and A. B. Fulton. 1987. Cotranslational assembly of myosin heavy chain in developing cultured skeletal muscle. *Proc. Natl. Acad. Sci. USA.* 84:6174–6178.
Jeffrey, W. 1982. Messenger RNA in the cytoskeletal framework: analysis by in situ hybridization. *J. Cell Biol.* 95:1–7.
Jeffrey, W. R. 1984. Spatial distribution of messenger RNA in the cytoskeletal framework of Ascidian eggs. *Dev. Biol.* 103:482–492.
Karpetsky, T. P., M. S. Boguski, and C. C. Levy. 1979. *In* Subcellular Biochemistry. D. E. Roodyn, editor. Plenum Press, New York. Vol. 6, 1–116.
Kish, V. M., and T. Pederson. 1976. Poly(A)-rich ribonucleoprotein complexes from HeLa cell messenger RNA. *J. Biol. Chem.* 251:5888–5894.
Kwan, S.-W., and G. Brawerman. 1972. A particle associated with the polyadenylate segment in mammalian messenger RNA. *Proc. Natl. Acad. Sci. USA.* 69:3247.
Lawrence, J. B., and R. H. Singer. 1986. Intracellular localization of messenger RNAs for cytoskeletal proteins. *Cell.* 45:407–415.
Lawrence, J. B., C. A. Villnave, and R. H. Singer. 1988. Sensitive, high-resolution chromatin and chromosome mapping in situ: presence and orientation of two closely integrated copies of EBV in a lymphoma line. *Cell.* 52:51–61.
Lawrence, J. B., R. H. Singer, and L. M. Marselle. 1989. Highly localized tracks of specific transcripts within interphase nuclei visualized by in situ hybridization. *Cell.* 57:493–502.
Lenk, R., and S. Penman. 1979. The cytoskeletal framework and poliovirus metabolism. *Cell.* 16:289–301.
Lenk, R., L. Ransom, Y. Kaufmann, and S. Penman. 1977. A cytoskeletal structure with associated polyribosomes obtained from HeLa cells. *Cell.* 10:67–78.
Luby-Phelps, K., and D. L. Taylor. 1988. Subcellular compartmentalization by local differentiation of cytoplasmic structure. *Cell Motil. Cytoskeleton.* 10:28–37.
Luby-Phelps, K., D. L. Taylor, and F. Lanni. 1986. Probing the structure of cytoplasm. *J. Cell Biol.* 102:2015–2022.
Manuelidis, L., P. R. Langer-Safer, and D. C. Ward. 1982. High-resolution mapping of satellite DNA using biotin-labeled DNA probes. *J. Cell Biol.* 95:619–625.
Munroe, D., and A. Jacobson. 1990. Tales of poly(A): a review. *Gene (Amst.).* 91:151–158.
Neilson, P., S. Goelz, and H. Trachsel. 1983. The role of the cytoskeleton in eukaryotic protein synthesis. *Cell Biol. Int. Rep.* 7:245–254.
Ornelles, D.A., E. G. Fey, and S. Penman. 1986. Cytochalasin releases mRNA from the cytoskeletal framework and inhibits protein synthesis. *Mol. Cell. Biol.* 6:1650–1662.
Pramanik, S. K., R. W. Walsh, and J. Bag. 1986. Association of messenger RNA with the cytoskeletal framework in rat L6 myogenic cells. *Eur. J. Biochem.* 160:221–230.
Pudney, J., and R. H. Singer. 1979. Electron microscopic visualization of the filamentous reticulum in whole cultured presumptive chick myoblasts. *Am. J. Anat.* 156:321–336.
Ramaekers, F. C. S., E. L. Benedetti, I. Dunia, P. Vorstenbosch, and H. Bloemendal. 1983. Polyribosomes associated with microfilaments in cultured lens cells. *Biochim. Biophys. Acta.* 740:441–448.
Sachs, A. B., and R. W. Davis. 1989. The poly(A) binding protein is required for poly(A) shortening and 60S ribosomal subunit-dependent translation initiation. *Cell.* 58:857–867.
Sachs, A. B., and J. A. Deardoff. 1992. Translation initiation requires the pAB-dependent poly(A) ribonuclease in yeast. *Cell.* 70:961–973.
Sachs, A. B., M. W. Bond, and R.D. Kornberg. 1986. A single gene from yeast for both nuclear and cytoplasmic polyadenylate-binding proteins: domain structure and expression. *Cell.* 45:827–835.
Sheiness, D., and J. E. Darnell. 1973. Polyadenylic acid segment in the mRNA becomes shorter with age. *Nature (Lond.).* 241:265–268.
Singer, R. H., G. L. Langevin, and J. B. Lawrence. 1989. Ultrastructural visualization of cytoskeletal mRNAs and their associated proteins using double-label in situ hybridization. *J. Cell Biol.* 108:2343–2353.
Sundell, C. L., and R. H. Singer. 1990. Actin mRNA localizes in the absence of protein synthesis. *J. Cell Biol.* 111:2397–2403.
Sundell, C. L., and R. H. Singer. 1991. Requirement of microfilaments in sorting of actin messenger RNA. *Science (Wash. DC).* 253:1275–1277.
Terasaki, M., J. Song, J. R. Wong, M. J. Weiss, and L. B. Chen. 1984. Localization of endoplasmic reticulum in living and glutaraldehyde-fixed cells with fluorescent dyes. *Cell.* 38:101–108.
Toh, B. H., S. J. Lolait, J. P. Mathy, and R. Baum. 1980. Association of mitochondria with intermediate filaments and of polyribosomes with cytoplasmic actin. *Cell Tissue Res.* 211:163–169.
Valenzuela, P., M. Quiroga, J. Zaldivar, W. J. Rutter, M. W. Kirschner, and D. W. Cleveland. 1981. Nucleotide and corresponding amino acid sequences encoded by alpha and beta tubulin mRNAs. *Nature (Lond.).* 289:650–655.
van Venrooij, W. J., P. T. G. Sillekens, C. A. G. van Eekelen, and R. J. Reinders. 1981. On the association of mRNA with the cytoskeleton in uninfected and adenovirus-infected human KB cells. *Exp. Cell Res.* 135:79–91.
Wolosewick, J. J., and K. R. Porter. 1979. Microtrabecular lattice of the cytoplasmic ground substance: artifact or reality. *J. Cell Biol.* 82:114–139.
Yang, F., M. Demma, V. Warren, S. Dharmawardhane, and J. Condeelis. 1990. Identification of an actin-binding protein from dictyostelium as elongation factor 1a. *Nature (Lond.).* 347:494–496.
Zumbe, A., C. Stahli, and H. Trachsel. 1982. Association of a M_r 50,000 cap-binding protein with the cytoskeleton in baby hamster kidney cells. *Proc. Natl. Acad. Sci. USA.* 79:2927–2931.